Seismic behavior of long-span arch culverts

Alper Turan Ph.D. PEng.
Ontario Ministry of Transportation, Material Engineering Research Office, Downsview, ON, Canada.

M. Hesham El Naggar, Ph.D. PEng.
Department of Civil and Environmental Engineering, the University of Western Ontario, London, ON, Canada.

2011 Pan-Am CGS Geotechnical Conference

ABSTRACT

Large span arch culvert (LSAC) structures have suffered minimum or no damage during past seismic events. This satisfactory seismic performance can largely be attributed to unique load distribution between the arch culvert and the surrounding engineered backfill. However, there are case histories documenting the failure of these structures under static loads due to asymetric load distribution along the culvert arch. The asymetric distribution of the backfill density and local loss of confinement around the arch may result in substantial servicability problems or even structural damage of arch culverts under static loads. This study focuses on the effect of backfill compaction on the distribution of seismic forces within the culvert-soil system. The study comprises static and dynamic explicit nonlinear finite difference analyses in order to account for large strains expected during strong earthquakes. The effects of soil structure interaction (SSI) on the ground motion as well as the effect of dynamic loading amplitudes on the arch's moments and thrusts are examined considering various compaction arrangements. It was found that SSI has a significant effect on the ground motions. The results indicated that significant increases in the moments and thrusts of LSAC may occur due to the seismic loads and the backfill arrangements can substaintially magnify these increases.

RÉSUMÉ

Grande durée de ponceau voûté (GDPV) structures ont subi au moins ou pas de dommages au cours des derniers événements sismiques. Cette performance satisfaisante sismique peut largement être attribuée à la répartition des charges unique entre le ponceau voûté et le remblai autour d'ingénierie. Cependant, il ya des histoires de cas qui documente l'échec de ces structures sous charges statiques dues à la répartition de la charge asymétrique le long de la voûte du ponceau. La répartition asymétrique de la densité de remblayage et de perte locale de confinement autour de l'arc peut entraîner des problèmes serviabilité importante, voire des dommages structuraux des ponceaux voûtés sous les charges statiques. Cette étude porte sur l'effet de compactage du remblai sur la répartition des forces sismiques dans le système de drainage-sol. L'étude comprend statique et dynamique non linéaire explicite des analyses de différences finies afin de tenir compte des grandes déformations attendus au cours de forts tremblements de terre. Les effets de l'interaction de la structure du sol (ISS) sur le mouvement du sol ainsi que l'effet des amplitudes de chargement dynamique des moments de l'arc et les orientations sont examinées compte tenu des dispositions de compactages différents. Il a été constaté qu'ISS a un effet significatif sur les mouvements du sol. Les résultats indiquent que des augmentations significatives dans les moments et les axes de GDPV peut se produire en raison des charges sismiques et les modalités de remblai peut substaintially magnifier ces augmentations.

1 INTRODUCTION

The seismic performance of LSAC has attracted little attention mainly due to the lack of reported seismic failures. Consequently, a few studies focussed on this topic and only a few design guidelines included general provisions on the seismic design of such structures. Fairless and Kirkcaldie (2008) provides a comprehensive literature review on the current research and design procedures.

Despite the significant number of studies performed on the seismic behaviour of buried structures, there is little reference to large span arch culverts. Davis & Bardet (2000) investigated the performance of 61 corrugated metal pipes (CMPs) during the 1994 Northridge earthquake in California. They concluded that flexible buried structures that are properly designed for static loads can resist the seismic accelerations in the order of 0.3g horizontal and 0.2g of vertical. Youd and Beckman (1996) studied the seismic performance of flexible culverts during the Alaska and Northridge earthquakes. They concluded that the culverts remained undamaged under peak ground acceleration (PGA) up to 0.5g. Fairless and Kirkcaldie (2008) indicated that failures and deformations observed in few occasions were due to slope instability, loss of soil stiffness, permanent ground deformation or settlement of embedding soil.

Byrne et al. (1996) investigated the seismic response of a 10.5 m span, 5.2 m rise concrete arch and reported significant increases in the arch's thrust and moment when the PGA was greater than 0.3g. They reported two distinct behaviours under the horizontal and vertical components of seismic loading: for horizontal shaking, the surrounding soil was much stiffer than the arch and the loads are taken by the soil rather than the arch; under vertical shaking, the

arch was stiffer than the surrounding soil and attracted significant loads. Allmark (2001) indicated that damage to cut and cover structures could be due to one of three conditions: inadequate lateral design strength, construction practice not reflecting design assumptions, and poor layout of construction or seismic joints.

The main objective of the present study is to examine the seismic behaviour of LSAC with a particular focus on soil non-linearity, SSI and backfill compaction.

2 CANADIAN DESIGN PRACTICES

The Canadian Highway Bridge Design Code, (CHBDC, 2006) addresses three different types of buried structures and their seismic design. These structures include soil-metal structures, metal box structures and concrete structures.

The CHBDC (2006) states that the horizontal and vertical components of the seismic ground shaking result in increased forces and moments in buried structures. The increase in thrust is largely controlled by the vertical component of the earthquake, while the increase in moment is largely controlled by the horizontal component of the earthquake (CHBDC, 2006). The vertical component of the earthquake acceleration, expressed as the vertical acceleration ratio, A_V, will effectively increase the unit weight of the soil from y to y $(1 + A_V)$. A_V can be taken as two-thirds of the horizontal acceleration ratio, A_H, which is equal to the zonal acceleration ratio, A, for the region of interest. The CHBDC specifies that buried concrete arch structures, as well as soil-metal and metal box structures, shall be designed considering additional seismic induced moments and thrusts. The specified additional seismic effects are described below.

2.1 Seismic design of soil-metal structures

The additional seismic induced thrust, T_E, for these structures are calculated as

$$T_E = T_D \,.\, A_V \qquad [1]$$

where, T_D is the thrust caused by the dead loads and A_V is the vertical acceleration ratio (2/3 of the horizontal acceleration ratio). The horizontal accelerations have little effect on thrust, which represents the basis for design of soil-metal structures with shallow corrugations. Hence, only T_E need be considered in these structures, and the factored thrust, T_f, for earthquake loading is given by:

$$T_F = (\alpha_D \,.\, T_D + T_E) \qquad [2]$$

where, α_D is dead load factor.

2.2 Seismic design of metal box structures

The affect of the horizontal earthquake component on the metal box structures is estimated by means of introducing additional seismic moments calculated as a proportion of the moments imposed by static loads. The additional seismic moments are calculated as:

$$M_E = M_D . A_V \qquad [3]$$

where, M_D is the moment caused by the dead loads and A_V is the vertical acceleration ratio (2/3 of the horizontal acceleration ratio). The seismic moments of the crown and haunch are factored using parameters κ and $(1-\kappa)$, respectively. The parameter κ is calculated as a function of culvert span, S as;

$$\kappa = 0.7 - 0.0328.S \qquad [4]$$

The total factored moments M_{CF} and M_{HF} including the earthquake effects are calculated as follows;

$$M_{CF} = \kappa.(\alpha_D \,.\, M_D + M_E) \qquad [5]$$

$$M_{HF} = (1-\kappa)\,(\alpha_D \,.\, M_D + M_E) \qquad [6]$$

2.3 Seismic design of concrete structures

The additional force effects due to earthquake loads are accounted for by multiplying the force effects due to the self-weight and earth loads times A_V.

3 METHODOLOGY

3.1 Problem Geometry

The LSAC considered in this study has a semi-circular reinforced concrete arch with width = 15 m, rise = 7.5 m, thickness = 0.3m, elastic modulus, E_c = $30x10^9$ Pa, Poisson's ratio = 0.25 and density = 2500 kg/m^3. A deep cover (see Figure 1) was considered as this approach eliminates the effects of the live loads on the moment/thrust of arch and simplifies the dynamic analysis procedure.

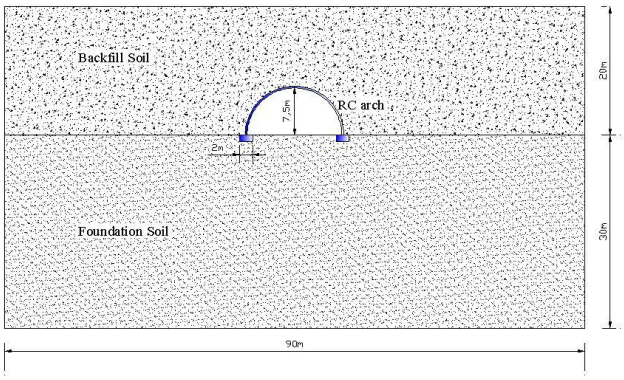

Figure 1 Schematic of problem geometry

3.2 Stratigraphy and Soil Properties

The ground stratigraphy considered in the analyses comprises two granular layers: a 30 m thick layer of very dense granular deposit of foundation soil; and a 20 m thick granular fill. Constant stiffness and strength profiles along the depth of layers are adopted for simplicity. Table 1 provides a summary of strength and stiffness properties of foundation soil and granular engineered backfill compacted in three different levels of compaction. Three degrees of compaction are considered to parametrically study the effect of backfill stiffness on SSI behavior. Thus, details of physical properties such as mass density and viod ratio are provided instead of compaction effort and procedures. The material properties in Table1 are estimated in accordance with Hardin and Richard (1963). Small strain moduli of the granular soils are calculated as follows;

$$G_0 = A.F(e).(\sigma_0')^n \qquad [7]$$

where, A and n are constants, σ_0' is the confining stress and $F(e)$ is the void ratio function.

In the present study an elastic-perfectly plastic stress–strain relationship with a Mohr–Coulomb failure criterion is adopted. For small shear strain levels, energy dissipation is achieved by viscous damping. Rayleigh damping is considered, consisting of two viscous components, stiffness proportional and mass proportional. The model natural frequency is determined from the undamped model oscillations generated as a result of instantaneously applied gravitational field. A central frequency is specified between the natural frequency of the model and the predominant frequency of the input motion.

The default hysteresis model, in which an S-shaped curve of modulus versus logarithm of cyclic strain are represented by a cubic equation, with zero slope at both low strain and high strain, is utilized in the analysis (Itasca, 2005). This hysteresis model is applied to all soil types. Figure 2 shows the hysteretic loops generated considering the above mentioned hysteresis model and cyclic strains ranging from 0.0001% to 1% applied on a single element of Backfill1. The hysteretic parameters are calibrated to provide the stiffness degradation and damping increase relationships presented in Seed and Idriss (1970) for sands.

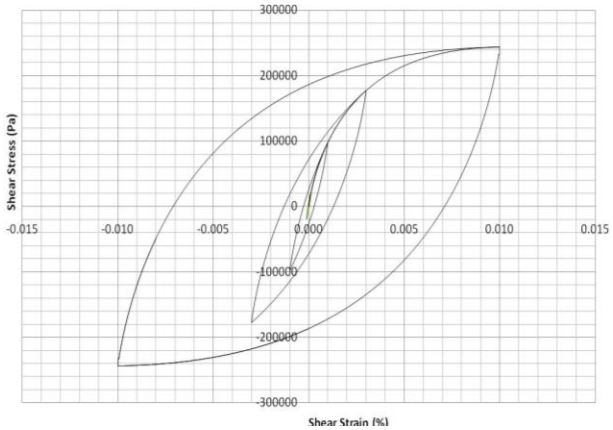

Figure 2 Hysteretic loops for Backfill1

3.3 Numerical Model and Boundary Conditions

The LSAC is supported on strip footing that would result in uniform settlement within tolerable ranges. It is also assumed that the foundation soil and soil beneath the soil column adjacent to the arch have similar deformation characteristics to avoid negative arching, which can result in an increase in thrust. This is done by assuming a less deformable foundation soil, simulating the construction staging and achieving the geostatic equilibrium prior to the construction of each backfill lift. The backfill is raised simultaneously in both sides of the arch.

Various backfill arrangements are considered in this study. The first arrangement (Case 1) comprised uniform backfilling of LSAC on each side using soil types Backfill1, Backfill2 and Backfill3. The second arrangement (Case 2) involves backfilling using Backfill1 and Backfill2 on the left and right sides of LSAC, respectively. In the third arrangement (Case 3), Backfill1 and Backfill3 are used on the left and right sides of the model, respectively. Table 1 summarizes the mechanical properties of granular backfills at various levels of compaction.

A plane strain explicit finite difference model was used. The arch was modelled using linear-elastic liner elements. The maximum element size used is 1/10th of the minimum Rayleigh wavelength in order to facilitate transmitting the higher frequency components of input motion (Kramer, 1996). Free-field boundaries that minimize the effect of reflecting

Table 1 Strength and stiffness properties of soils

Material Type	Mass Density (kg/m^3)	Shear Modulus (MPa)	Shear Wave Velocity (m/s)	void ratio	Poisson's Ratio	Angle of Friction (o)	Rayleigh Damping Ratio (%)
Foundation Soil	2200	1000	700	N/A	0.3	38	5
Backfill 1	2000	240	346	0.35	0.3	36	5
Backfill 2	1800	173	310	0.5	0.3	35	5
Backfill 3	1600	114	267	0.7	0.3	33	5

waves from the vertical model boundaries, and simulate the behaviour of soil medium extending to infinity using a 1-D soil column, are utilized.

3.4 Static and Dynamic Loads

The static loads considered are the gravitational loads that result from the backfilling of the LSAC and the fill on top of the crown.

The dynamic loads are modelled as an acceleration time history applied to the base of the model. A Ricker wavelet is used as acceleration input time history which is described as:

$$a(t) = A.\frac{1-2[\pi.f.dt.(t-t_0)]}{\exp[[\pi.f.dt.(t-t_0)]^2]} \qquad [8]$$

where, *a(t)* is the acceleration time history, *t* is the time, *dt* is the time sampling interval, t_0 is the duration of interest, *A* is the maximum acceleration amplitude, and *f* is the predominant frequency of the motion. The horizontal seismic loading conditions are simulated using Ricker wavelets with three levels of peak amplitudes, 0.1g, 0.2g and 0.3g, in order to model different levels of non-linear soil behaviour. The duration and predominant frequency of the loading are selected as 4 seconds and 1 Hz, respectively. Figure 3 gives the acceleration time histories derived using Eq. 8 for three levels of peak acceleration amplitudes.

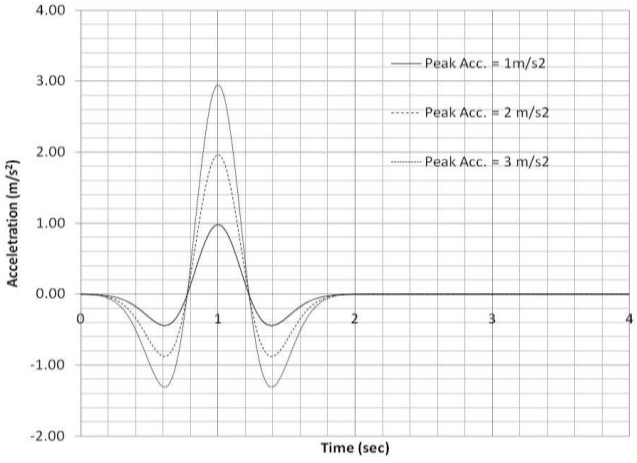

Figure 3 Ricker wavelets used in analyses

3.5 Analyses

The analysis procedure involved a number of steps. An initial static analysis, which followed a typical construction sequence, is performed in order to establish geostatic equilibrium. The seismic analysis is then performed for each case. The seismic loading is simulated by applying acceleration time histories at the base of the model. Fairless and Kirkcaldie (2008) indicated that the ability of soil-arch culvert interface to slip/separate has almost no effect on dynamic deformations, including the amount of racking during shaking and fully bonded interface assumption causes larger seismic reactions at the footings. Thus, the analyses are performed considering fully bonded soil structure interface, which sets a more critical case. The static stiffness values are assumed to be 1/3th of the dynamic stiffness values reported in Table 1.

Static Analyses

The analytical method outlined in the CHBDC (2006) represents the seismic forces and moments as a function of static values. Determination of initial static conditions is critical for an appropriate SSI evaluation of the LSAC. The static analyses are conducted considering construction sequence.

Dynamic Analyses

The dynamic analyses are preferred over pseudo-dynamic analyses in order to evaluate amplification, phasing, seismic induced displacements, thrusts and moments more realistically (Byrne et al, 1996).

Initially, the free field ground response of the soil is determined using a 2D model excited by the dynamic loads shown in Fig. 3. Subsequently, a series of 2D SSI analyses of the LSAC are conducted. Only horizontal dynamic excitations are applied; however, resultant vertical vibration components generated due to amplification, phasing and SSI are also monitored and discussed within this study.

4 RESULTS AND DISCUSSIONS

4.1 Ground Response and SSI

Figure 4 shows a schematic comprising the reference points at which various quantities are monitored.

Free Field Response

The results of free field analyses suggest that the horizontal PGA with levels of 0.1g, 0.2g and 0.3g, are amplified from the model base to the ground surface, with amplification factors (A_f) for Case 1 (Backfill 1) of 1.40, 1.38 and 1.33, respectively. At PGA of 0.1g, the soil behaviour was almost linear elastic. However, as the PGA increased, non-linear increase of hysteretic damping and degradation of dynamic stiffness took place, which resulted in decreasing A_f. The soil profiles in Case 1 (Backfill2) and Case 1 (Backfill3) amplified the ground motion (PGA = 0.3g) with A_f of 1.71 and 2.59, respectively.

The free field vertical accelerations at the ground surface are calculated as 0.26g, 0.36g and 0.39g for Case 1 (Backfill1) Case 1 (Backfill2) Case 1 (Backfill3) ground profiles. These values are

calculated for a horizontal input ground motion of with a PGA of 0.3g.

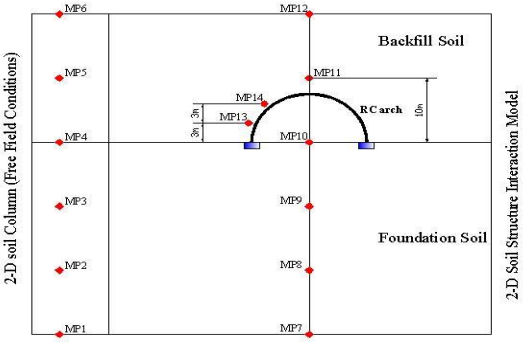

Figure 4 Schematic of the reference points

Response of SSI System

The results showed that SSI resulted in significant alteration to both horizontal and vertical ground motions. Figure 5 compares amplification factors at free field and at the centerline of the LSAC for Case 1 (Backfill1). The A_f at MP11 and MP12 are48% and 22% compared to free field amplification. Vertical accelerations at MP11 increased approximately 200%, but remained almost unchanged at MP12.

Tables 2 and 3 present the results of SSI analyses considering three different symmetric backfilling arrangements. The results shown in Table 2 indicate that the horizontal ground motions are amplified at the free field and at the centerline for all three backfill arrangements, but A_f values are generally higher at the centerline. This difference is higher above the crown. The A_f values at MP11 are higher than free field values by47%, 35% and -6% forBackfill1, Backfill2) and Backfill3. The results indicate that the sudden increase of horizontal accelerations above the crown is more pronounced for Case 1 (Backfill1).

The results shown in Table 3 indicate that the vertical ground motions are also amplified at the free field and at the centerline for all three backfill arrangements. The vertical accelerations at the centerline are generally higher than those in the free field. This difference is significantly high (200%) at immediately above the crown for Case 1 (Backfill1). The difference is calculated as 35% and -25% for Case 1 (Backfill2) and Case 1 (Backfill3), respectively.

Figure 6 shows the variation of cyclic shear strains at the haunch and the crown of LSAC. Results indicate that the shear strains occurred at the haunch (MP13) is five times larger than those occurred in the crown for all three levels of backfill compaction. The results show that the shear strains occurred at Case 1 (Backfill1) is recoverable. However, irrecoverable shear strains occurred both at the haunch and the crown for Case 1 (Backfill2) and Case 1 (Backfill3). The increasing magnitude of shear strains from Case 1 (Backfill1) to Case 1 (Backfill3) is due to the increasing soil non-linearity caused by lower soil strength and stiffness and hysteretic soil non-linearity.

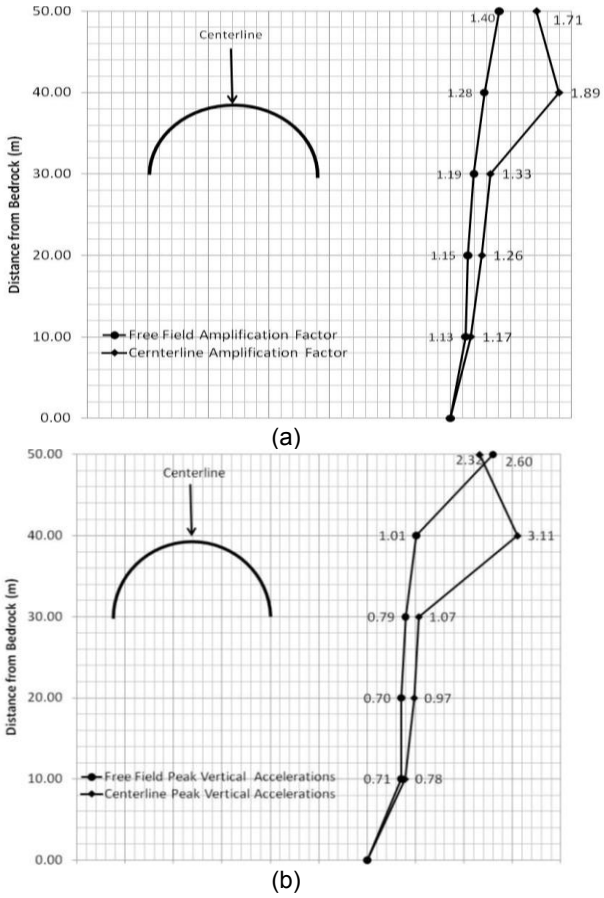

Figure 5 Effect of SSI on the (a) horizontal amplification factors, (b) vertical accelerations

Tables 2 and 3 present the results of SSI analyses considering three different symmetric backfilling arrangements. The results shown in Table 2 indicate that the horizontal ground motions are amplified at the free field and at the centerline for all three backfill arrangements, but A_f values are generally higher at the centerline. This difference is higher above the crown. The A_f values at MP11 are higher than free field values by 47%, 35% and -6% forBackfill1, Backfill2) and Backfill3. The results indicate that the sudden increase of horizontal accelerations above the crown is more pronounced for Case 1 (Backfill1).

The results shown in Table 3 indicate that the vertical ground motions are also amplified at the free field and at the centerline for all three backfill arrangements. The vertical accelerations at the centerline are generally higher than those in the free field. This difference is significantly high (200%) at immediately above the crown for Case 1 (Backfill1). The difference is calculated as 35% and -25% for

Case 1 (Backfill2) and Case 1 (Backfill3), respectively.

Figure 6 shows the variation of cyclic shear strains at the haunch and the crown of LSAC. Results indicate that the shear strains occurred at the haunch (MP13) is five times larger than those occurred in the crown for all three levels of backfill compaction. The results show that the shear strains occurred at Case 1 (Backfill1) is recoverable. However, irrecoverable shear strains occurred both at the haunch and the crown for Case 1 (Backfill2) and Case 1 (Backfill3). The increasing magnitude of shear strains from Case 1 (Backfill1) to Case 1 (Backfill3) is due to the increasing soil non-linearity caused by lower soil strength and stiffness and hysteretic soil non-linearity.

4.2 Seismic Induced Moments and Thrusts

Symmetrically Backfilled LSAC

The seismic induced moments and thrusts are presented for PGAs of 0.1g, 0.2g and 0.3g and three symmetric backfill arrangements. Figure 7 shows the seismic induced moment normalized by the maximum static moment for the three PGA values. Figure 7a indicates that the moments in the LSAC increase as the PGA increases. The maximum seismic induced moments are calculated as 1.5, 2.3 and 3.9 times the static moments for the PGA values. Figure 7b shows that the seismic moments are larger for less compacted backfill. The maximum seismic moments are 3.9, 5.1 and 8.5 times the static moments for Backfill1, Backfill2 and Backfill3, respectively.

Figure 8 shows the seismic thrusts normalized by the maximum static thrusts for the three PGA values. Figure 8a indicates that the thrusts in the LSAC increased as PGA increased. The maximum seismic induced moments are calculated as 1.2, 1.6 and 2.1 times the static thrusts for the PGAs of 0.1g, 0.2g and 0.3g, respectively. The results in Figure 8 (b) show that the thrusts in the LSAC reduce as the level backfill compaction reduces. The maximum seismic induced thrusts are calculated as 2.1, 1.9 and 1.7 times the static thrusts for Backfill1, Backfill2 and Backfill3, respectively.

Table 2 Effect of SSI on ground motions (Horizontal Accelerations)

	Case1 (Backfill1)			Case1 (Backfill2)			Case1 (Backfill3)		
Elevation	Free Field Horizontal Af	Centerline Horizontal Af	Difference	Free Field Horizontal Af	Centerline Horizontal Af	Difference	Free Field Horizontal Af	Centerline Horizontal Af	Difference
50.00	1.40	1.71	21.77%	1.71	1.93	12.64%	2.59	2.19	-15.40%
40.00	1.28	1.89	47.97%	1.37	1.86	35.29%	2.20	2.07	-5.97%
30.00	1.19	1.33	11.31%	1.16	1.30	12.09%	1.20	1.22	2.08%
20.00	1.15	1.26	10.09%	1.15	1.21	5.51%	1.15	1.25	8.61%
10.00	1.13	1.17	3.88%	1.14	1.18	3.16%	1.09	1.17	7.15%
0.00	1.00	1.00	0.00%	1.00	1.00	0.00%	1.00	1.00	0.00%

Table 3 Effect of SSI on ground motions (Vertical Accelerations)

	Case1 (Backfill1)			Case1 (Backfill2)			Case1 (Backfill3)		
Elevation	Free Field Vertical Acc. (m/s^2)	Centerline Vertical Acc. (m/s^2)	Difference	Free Field Vertical Acc. (m/s^2)	Centerline Vertical Acc. (m/s^2)	Difference	Free Field Vertical Acc. (m/s^2)	Centerline Vertical Acc. (m/s^2)	Difference
50.00	2.60	2.32	-10.61%	3.63	2.80	-22.97%	3.87	4.25	9.96%
40.00	1.01	3.11	207.65%	2.27	3.06	34.85%	4.27	3.19	-25.20%
30.00	0.79	1.07	35.02%	0.69	1.14	64.59%	0.92	1.05	13.88%
20.00	0.70	0.97	38.97%	0.66	0.87	32.17%	0.75	0.63	-16.21%
10.00	0.71	0.78	10.82%	0.67	0.77	14.77%	0.85	0.68	-19.30%
0.00	0.00	0.00	0.00%	0.00	0.00	0.00%	0.00	0.00	0.00%

Asymmetrically Backfilled LSACs

Figure 9 shows the effect of asymmetric backfill compaction on the seismic moments and thrusts for PGA of 0.3g. It is noted from Figure 9 that the asymmetric backfilling resulted in an increase in the seismic moments at the haunches and a decrease near the crown. These variations are calculated as high as 20% between the symmetric Case 1 and asymmetric Case 3. Asymmetric backfilling has a reducing affect on the seismic induced thrusts at the crown and both haunches of LSAC. Results showed

that this reduction is more pronounced at the right side of the LSAC, where the backfill was compacted to a lesser degree (Backfill3).

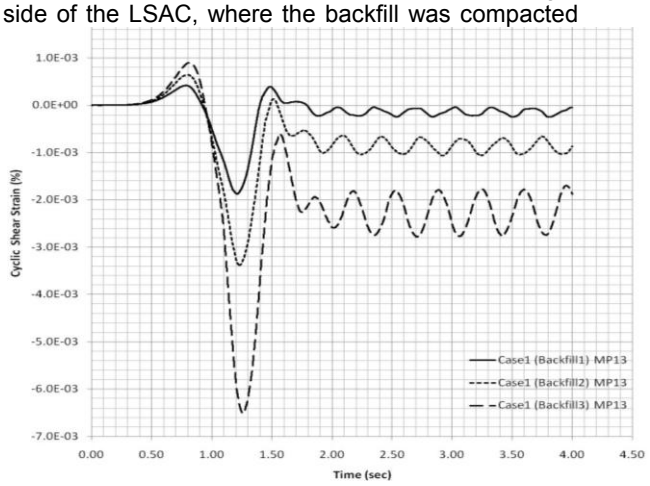

(a)

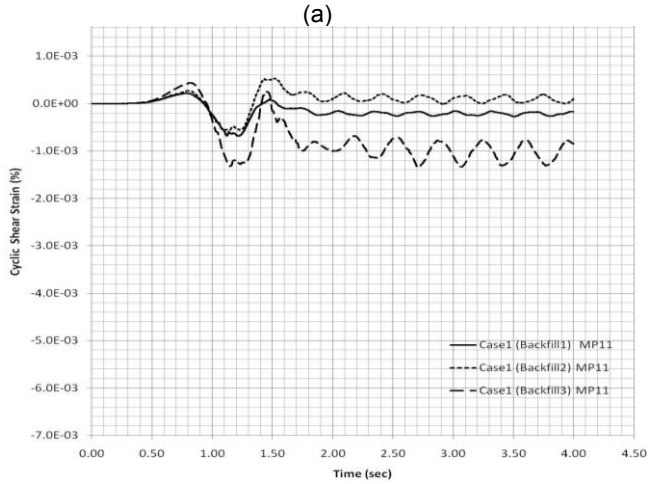

(b)

Figure 6 Cyclic shear strains at (a) haunch (b) crown

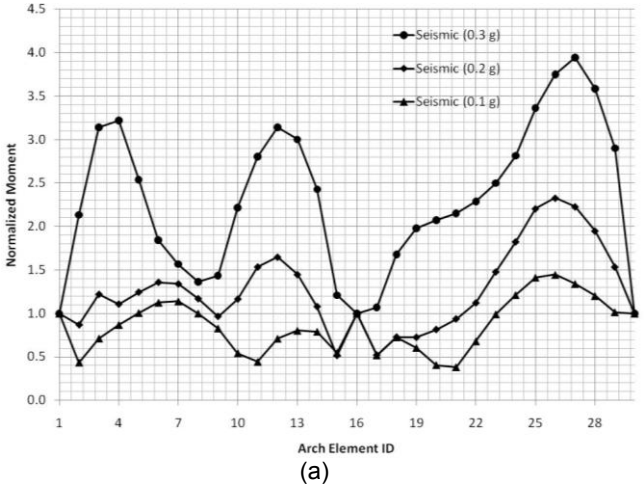

(a)

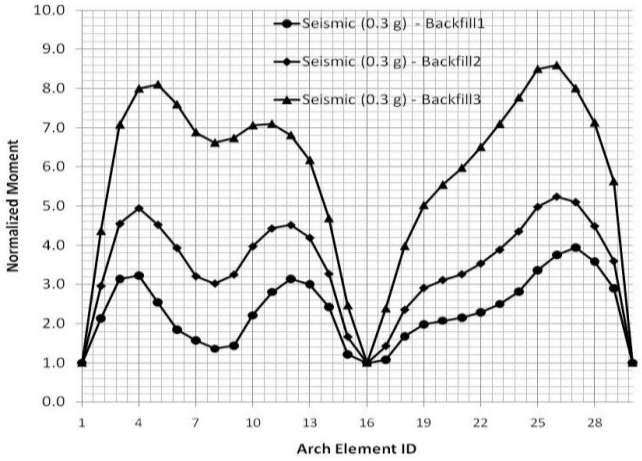

(a)

Figure 7 Normalized seismic moments vs. a) PGA b) backfill type

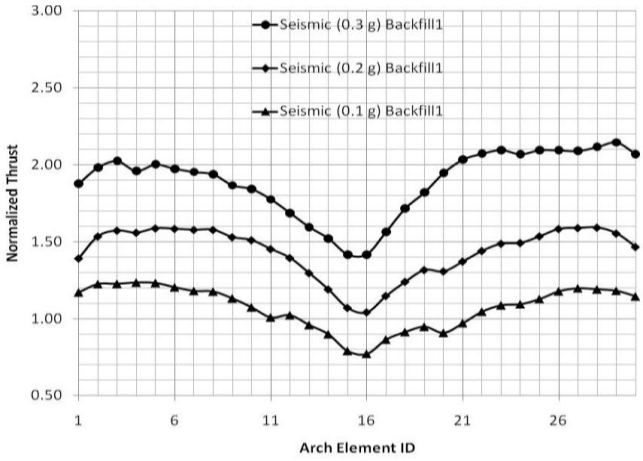

(a)

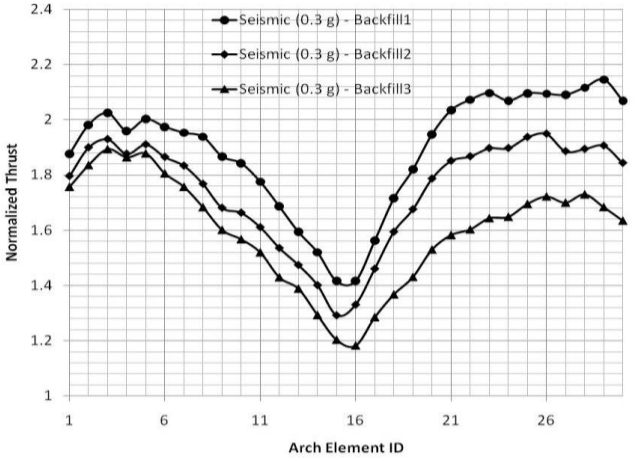

(b)

Figure 8 Normalized seismic thrust vs. a) PGA b) backfill type

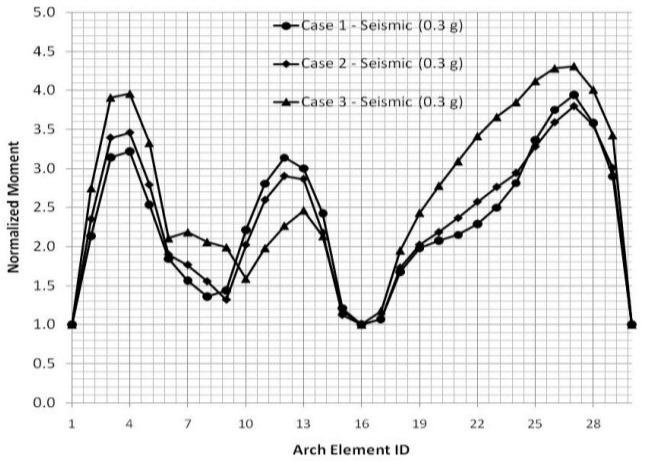

(a)

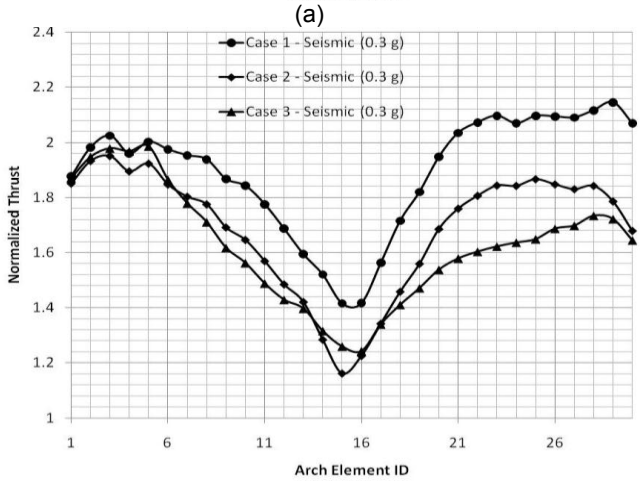

(b)

Figure 9 Normalized seismic a) moments b) thrusts for various asymmetric backfill cases

5 SUMMARY AND CONCLUSIONS

The seismic behaviour of LSACs is investigated considering the effects of ground motion amplitude, SSI, soil nonlinearity, and various backfill compaction arrangements. The following is a summary of the results.

- The results showed that the input ground motions are amplified through the soil profile at the free field by about 40% for the LSAC configuration considered.
- The ground motion with a PGA of 0.3g is amplified at the free field as the level of backfill compaction is reduced. A_f values increased by as high as 259% for loose backfill.
- The SSI resulted in significant alterations to both horizontal and vertical ground motions. Horizontal A_f increased as high as 47% relative to free field ground motions, while vertical accelerations increased by about 200% above the crown.
- Significant nonlinear soil behaviour occurred near the haunches, whereas the soil near the crown experienced relatively lower amplitudes of cyclic shear strain.
- The seismic moments increased as PGA increased for symmetric backfill. The maximum seismic moments are as high as 3.9 times the static moments for symmetric backfilling for PGA of 0.3g. The seismic moments are sensitive to the backfill compaction. The maximum seismic moments are 3.9, 5.1 and 8.5 times the static moments for symmetric backfilling with different levels of compaction.
- The seismic thrusts increased as PGA increased. The maximum seismic thrusts are calculated as 1.2, 1.6 and 2.1 times the static thrusts for symmetric backfilling (Backfill1) and the PGAs of 0.1g, 0.2g and 0.3g, respectively. The results show that the seismic thrusts decreased for less compact backfill.
- The asymmetric backfilling resulted in an increase of the seismic moments at the haunches and a decrease near the crown. The maximum variation of moments relative to symmetrically backfilled case remained at 20%. The seismic thrusts are reduced as a result of asymmetric backfilling.

ACKNOWLEDGEMENTS

The research reported in this paper has been partially supported by the Ontario Ministry of Transportation.

REFERENCES

Allmark, T. 2001. The Observed Damage to Buried Structures. *Newsletter of the Society. For Earthquake & Civil Engineering Dynamics (UK)*, Vol 14 No 4: 2–3.

Byrne, P.M, Anderson, D.L., Jitno, H. 1996. Seismic Analysis of Large Buried Culvert Structures. *Transportation Research Record* 1541: 133–139.

Canadian Highway Bridge Design Code, 2006. *Canadian Standards Association* CSA-S6-06.

Davis, C.A., Bardet J.P. 2000. Responses of Buried Corrugated Metal Pipes to Earthquakes. *Journal of Geotechnical and Geoenvironmental Engineering*, ASCE 126:28–39.

Fairless, G.J., and Kirkcaldie, D. 2008. Earthquake Performance of Long-Span Arch Culverts, *NZ Transport Agency Research Report 366.*

Hardin, B.O., and Richard, F.E., 1963. Elastic Wave Velocities in Granular Soils, *Journal of Soil Mechanics and Foundations.* ASCE, 89, SM1, 33-65.

Itasca Consulting Group (2005). FLAC, Fast Lagrangian Analysis of Continua, Version 5.0, Itasca Consulting Group, Minneapolis, Minnesota.

Kramer, S.L. (1996). Geotechnical Earthquake Engineering, Prentice-Hall Inc., Englewood Cliffs, N.J.

Seed, H. Bolton, and I. M. Idriss. “Soil Moduli and Damping Factors for Dynamic Response Analysis,” Earthquake *Engineering Research Center, University of California, Berkeley*, Report No. UCB/EERC-70/10, p. 48, Dec. 1970.

Youd, T.L., Beckman, C.J. 1996. Highway Culvert Performance During Past Earthquakes. National Center for Earthquake Engineering Research. Rep. NCEER-96-0015. Buffalo, NY